Real-time *in situ* fluorescence study of α-6T thin film growth on muscovite mica

Robert Zimmerleiter, Michael Hohage, and Lidong Sun [*]

Institute of Experimental Physics, Johannes-Kepler University Linz, Altenbergerstraße 69, Linz 4040, Austria

In this work, the findings of an *in situ* fluorescence spectroscopy and microscopy investigation of the growth of α-sexithiophene (α-6T) thin films on muscovite mica are presented. The sensitive dependence of the fluorescence emission on the molecular arrangement is exploited to reveal the details of the α-6T thin film growth from the initial stage. A Stranski-Krastanov growth mode with a two-monolayer-thick wetting layer is observed. The molecules within the wetting layer lie flat on the mica surface and their molecular arrangement evolves as a function of the surface coverage. After the completion of the wetting layer, needlelike three-dimensional islands consisting of flat-lying molecules and flat islands containing nearly-upright-standing molecules grow competitively. Exposing the α-6T thin films to air leads to dewetting and this process is found to be partially reversible, i.e., a large fraction of the wetting layer recovers gradually after the sample is transferred back into vacuum. This dewetting (rewetting) process is attributed to the surface modification due to the adsorption (desorption) of water molecules.

I. INTRODUCTION

Conjugated organic materials have attracted considerable interest due to their increasing application in electronic and optoelectronic devices [1,2]. In particular, the growth of highly oriented crystalline films is essential for improving the performance of organic thin film devices [3–5]. For this purpose, it is very important to understand the details of the nucleation and growth in order to manipulate the molecular arrangement and orientation accordingly [3,6–10]. In this context, it is highly desired to monitor the nucleation and growth *in situ* and in real time. In fact, great efforts have been made to realize this target using a wide range of experimental methods, including x-ray diffraction [11,12], photoelectron emission microscopy [13–15], low-energy electron microscopy [16–18], optical spectroscopy [19,20], and optical microscopy [21].

Fluorescence emission is characteristic of conjugated molecules relevant for optoelectronic device applications. Most importantly, the details of the emission are not only determined internally by the molecular structure, but also strongly influenced externally by the static and resonant electronic interactions [22]. This property makes fluorescence emission from organic molecules an attractive probe to identify molecules, determine their molecular orientation, and evaluate molecule-molecule and molecule-substrate interactions. Indeed, fluorescence microscopy has been applied to investigate the optical properties and molecular orientations of organic nanostructures synthesized on insulating substrates [23]. Laser scanning confocal microscopy has also been used to characterize ultrathin α-sexithiophene (α-6T) films deposited on SiO_2 substrates. The spatially resolved fluorescence spectroscopy reveals not only the morphology, but also the correlated optical properties, which in turn are extremely sensitive to the orientation and aggregation of the molecules in the film [24,25]. Recently, spatially resolved photoluminescence was used to study the early stage of crystallization of rubrene thin films on mica substrates. The spontaneous evolution of morphology and the local photoluminescence revealed that crystallization occurs when the amorphous islands coalesce and needlelike crystalline fibers are formed in the gap between the islands [26]. Most recently, complex organic nanostructures, i.e., periodic para-hexaphenyl (*p*-6P)/α-6T multilayer heterostructures, were investigated using spatially resolved fluorescence spectroscopy. The fluorescence spectroscopy showed that the emission from α-6T molecules at the interface with the substrate and three-dimensional (3D) crystallites is distinctive, demonstrating its sensitive dependence on the detailed arrangement of molecules in the nanostructures. Furthermore, the overall fluorescence emission of these organic multilayer nanostructures is dominated by a resonant energy transfer from *p*-6P to α-6T molecules at interfaces [27]. The success of these investigations suggests that a combination of fluorescence microscopy and spectroscopy will be a powerful tool for the *in situ* study of organic thin film growth. Additionally, it also allows the investigation on insulating substrates. However, in spite of all this progress achieved *ex situ*, no *in situ* real-time fluorescence microscopy study of organic thin film growth has been reported so far.

In this work, the intense florescence of α-6T is exploited to investigate the growth of α-6T thin films on muscovite mica *in situ* under ultrahigh-vacuum conditions by means of fluorescence microscopy and fluorescence spectroscopy. Actually, many studies on the growth of α-6T thin films on muscovite mica have already been published [28–30]. It has been shown that α-6T crystallizes on muscovite mica into the so-called low-temperature phase (LT) [31]. Two kinds of 3D islands referred to as needlelike and island-shaped configurations associated with 3D crystals with a ($\bar{4}$11) and

---

[*]lidong.sun@jku.at

a (100) contact plane with the surface have been revealed, respectively [30]. Furthermore, needlelike islands tend to grow along four well defined azimuths on muscovite mica and the long axis of the α-6T molecules within these islands are aligned accordingly [28–30]. Concerning the early stage of the α-6T thin film growth, there are still several open questions. For instance, it has been suggested that an α-6T wetting layer may form on muscovite mica, but no experimental evidence has been obtained. The only *in situ* measurement using low-energy electron diffraction revealed no additional diffraction peak related to the lattice of α-6T on the surface [29]. Consequently, the details of the nucleation and growth of this prototype system remain unclear. The current real-time *in situ* fluorescence study performed during the deposition of α-6T evidences the formation of a wetting layer at the initial stage of growth. In addition, a 2D phase transition has also been revealed as a function of the surface coverage of the wetting layer.

II. EXPERIMENT

α-6T molecules (Tokyo Chemical Industry Co. Ltd.) were deposited in ultrahigh-vacuum conditions with a base pressure of below 10^{-9} mbar from a Knudsen-type evaporator (Dr. Eberl MBE-Komponenten GmbH). The deposition rate was measured with a water-cooled quartz microbalance (Intellimetrics IL150) and amounted to approximately 1.7×10^9 molecules s^{-1} mm^{-2} which equals to $(9.1 \pm 0.6) \times 10^{-3}$ Å s^{-1}. This deposition rate was obtained by using the density of α-6T (1.553 g cm^{-3}) calculated from its molar mass and the dimensions of the unit cell of the LT-phase α-6T crystal. Before deposition, the α-6T molecules were heated to sublimation temperature (160 °C) in ultrahigh vacuum for about 2 h in order to remove impurities and water.

As the substrate, grade V-1 muscovite mica (Structure Probe, Inc.) with a thickness of 0.06 ± 0.01 mm was used. Muscovite mica is a sheet silicate that is often used as a substrate for vapor deposition studies due to its reasonable thermal stability up to 700 °C [32] and chemically inert nature. Each sheet of the muscovite structure consists of three layers where an octahedral layer of mostly aluminium is sandwiched between two identical tetrahedral layers with the composition $(Si, Al)_2O_5$ [33]. A partial cation substitution of Al^{3+} instead of Si^{4+} in the tetrahedral layers creates uncompensated charges which are balanced by a cation interlayer of potassium atoms between these sheets [30,34]. The muscovite mica can be easily cleaved along the (001) plane in the potassium layer, which was done in air prior to the measurements to get an atomically clean surface. Immediately after cleaving, the substrate was transferred into the vacuum chamber and its temperature was kept overnight at the growth temperature, namely, 400 K, using a proportional-integral-derivative controller to ensure a stable temperature can be reached and maintained before deposition.

In order to obtain fluorescence microscopy images and fluorescence spectra, a wide-field epifluorescence setup as shown in Fig. 1 was used, for which a commercially available Nikon D-FL-E microscope was attached to the vacuum chamber. The α-6T molecules adsorbed on the substrate surface are excited by a blue laser (Toptica Photonics AG)
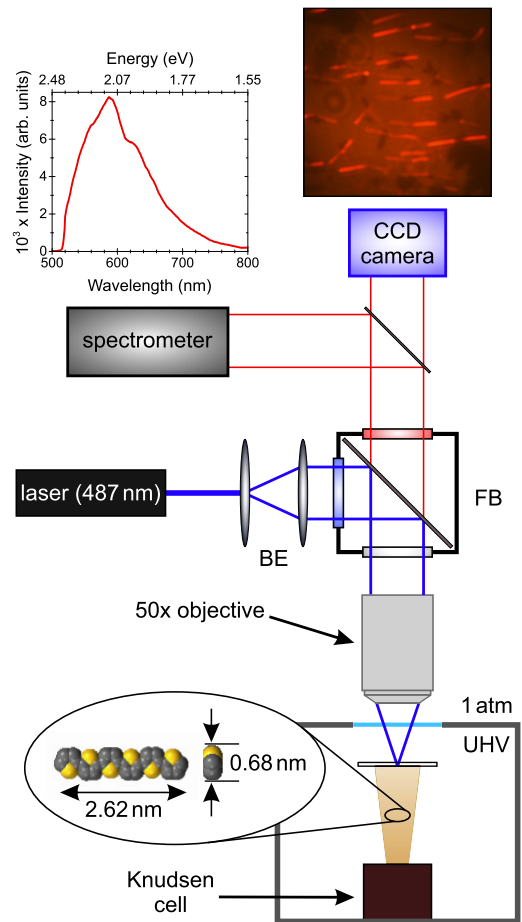

FIG. 1. Schematic drawing showing the epifluorescence setup used for the real-time *in situ* fluorescence study during the deposition of α-6T molecules on the transparent mica substrate. The structure of the α-6T molecule is shown in the ellipse.

with a wavelength of 487 nm and a maximum output power of 100 mW. In order to avoid photobleaching, the actual output power was limited to 0.7 mW during experiments. The initially linearly polarized laser beam first goes through a beam expander (BE) with a built-in quarter waveplate to obtain a circularly polarized beam before it enters a Nikon B2A filter block (FB). Due to its short wavelength, the beam passes the excitation filter and gets reflected by the built-in dichroic mirror which directs it into a $50\times$ objective (numerical aperture equal to 0.55). Passing through the transparent muscovite mica substrate, the laser beam is then focused at the front surface of the substrate which is exposed directly to the α-6T molecular beam. The spot size of the laser beam formed on the surface was approximately equal to 100 μm (FWHM). The fluorescence light emitted from the α-6T molecules on the surface was then collected by the same objective. Afterward it passes the dichroic mirror in the B2A filter block and the subsequent emission filter before finally being detected by a color CCD camera (Zeiss AxioCam HRc) and a high-performance spectrometer (Ocean Optics QEPro) simultaneously. The spectrometer is equipped with a Hamamatsu scientific grade back-thinned 1044×64 element CCD array and is TE cooled achieving a high quantum yield
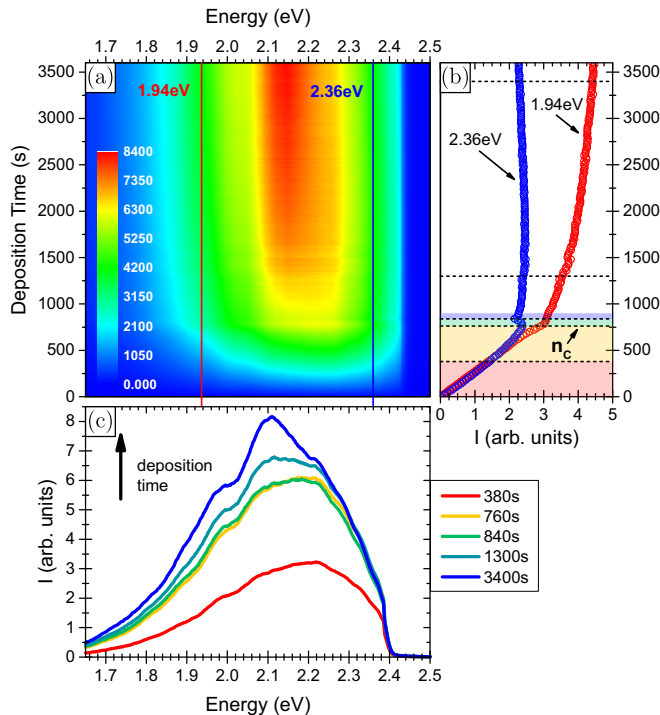
FIG. 2. (a) Contour plot showing the time evolution of the fluorescence intensities in an energy range between 1.65 and 2.50 eV during the depsoiton of α-6T. (b) Fluorescence intensities at 2.36 eV (blue) and 1.94 eV (red) plotted as a function of the deposition time. The areas colored with red, yellow, green, and blue cover the first four growth stages (see the text), respectively. The horizontal dashed lines represent the times when the spectra presented in (c) were recorded. (c) Fluorescence spectra recorded at the time indicated by the horizontal dashed lines in (b), representing the characteristic spectra for each growth stage.

of 90%. The laser illumination was limited to 2.5 s for every 20 s to avoid photobleaching effects. Reference measurements have been conducted to confirm that with the selected laser power and exposure time the influence on the fluorescence of the molecules is negligible.

III. RESULTS AND DISCUSSION

A. *In situ* study during the growth of α-6T thin films

A contour plot showing the fluorescence intensity recorded *in situ* during the deposition of α-6T is shown in Fig. 2(a). The total deposition time was 3600 s, which gives a nominal thickness of approximately 3.3 nm for the final α-6T thin film. The fluorescence intensities within a wavelength range from 1.65 to 2.50 eV are shown. The cutoff wavelength of the used Nikon B2A filter block is about 2.40 eV, which explains the sharp edge visible on the left side of the plot. The observed fluorescence is due to the relaxation of the highest occupied molecular orbital (HOMO) to lowest unoccupied molecular orbital (LUMO) excitation of α-6T molecules. The direction of the corresponding transition dipole moment is parallel to the long molecular axis of α-6T. The emission intensity and its energetic distribution depend strongly on the molecular interaction [24,25,35]. Consequently, noninteracting molecules

and molecular crystals emit distinctive characteristic spectra [24,25,35]. From the forthcoming discussion about the characteristic spectral line shape of α-6T thin films at the different growth regimes, it will become clear that the fluorescence intensity at 2.36 and 1.94 eV are sensitive probes to the wetting layer and 3D islands, respectively. It is worth pointing out that the purpose of selecting 2.36 eV instead of the exact peak position as the characteristic wavelength of the wetting layer is to minimize the interruption from the fluorescence intensity of 3D islands. Therefore, the variation of the fluorescence intensity at 2.36 eV (blue circles) and at 1.94 eV (red circles) is plotted as a function of the deposition time in Fig. 2(b). Furthermore, the fluorescence spectra recorded at several selected deposition times indicated by the dashed horizontal lines in Fig. 2(b) are presented in Fig. 2(c).

Based on the spectral evolution of the fluorescence emitted from the α-6T thin film, the growth can be separated into two parts by a deposition time of about 840 s, namely, wetting layer growth and 3D island growth regime, respectively. The characteristic spectral line shape of the fluorescence from the α-6T thin film in the wetting layer regime is similar to that of noninteracting α-6T molecules [24,25,35] with its maximum located around 2.21 eV (see Fig. S1 in [36]). The intensity of the corresponding fluorescence signal increases as a function of the deposition time. This observation indicates that both molecule-molecule and molecule-substrate interactions [37–40] are rather weak, suggesting the α-6T molecules are lying flat on the mica surface. Further deposition induces two new sharp emission features at ~1.93 eV and ~2.10 eV which stem from the characteristic fluorescence spectrum from α-6T crystals in the LT phase [24,25,41] (see Fig. S2 in [36]). This observation implies the growth of α-6T crystals after the completion of the wetting layer and consequently that the α-6T growth on the mica follows the Stranski-Krastanov mode. This conclusion will become even more clear after the forthcoming discussion of the *in situ* fluorescence images recorded during the growth of the α-6T thin film.

With closer inspection of the evolution of the fluorescence signals plotted in Fig. 2(b), one can recognize that the growth of the wetting layer can be further divided into three stages [indicated by the red, yellow, and green areas in Fig. 2(b)]. This can be seen even more clearly in Fig. 3, where the incremental changes of the fluorescence spectrum upon the growth of the α-6T thin film within given time intervals are shown. Therein the change of the fluorescence is presented in two ways. (i) In the top row of Fig. 3, the changes of the fluorescence image over the duration of each growth stage (obtained by subtracting the fluorescence image recorded at the end from the one taken at the beginning of the corresponding growth stage) are presented. (ii) In the middle row of Fig. 3, the incremental changes of the fluorescence spectrum during the indicated time intervals are plotted. In order to gain a better understanding of the growth mechanism, each growth stage will be discussed separately in the following sections.

1. *Growth stage I: First-monolayer growth (0–38 s)*

The first stage corresponds to the initial linear increase of the fluorescence intensity at both 2.36 eV (blue) and 1.94 eV (red) in Fig. 2(b) before the splitting of the two curves at 380 s
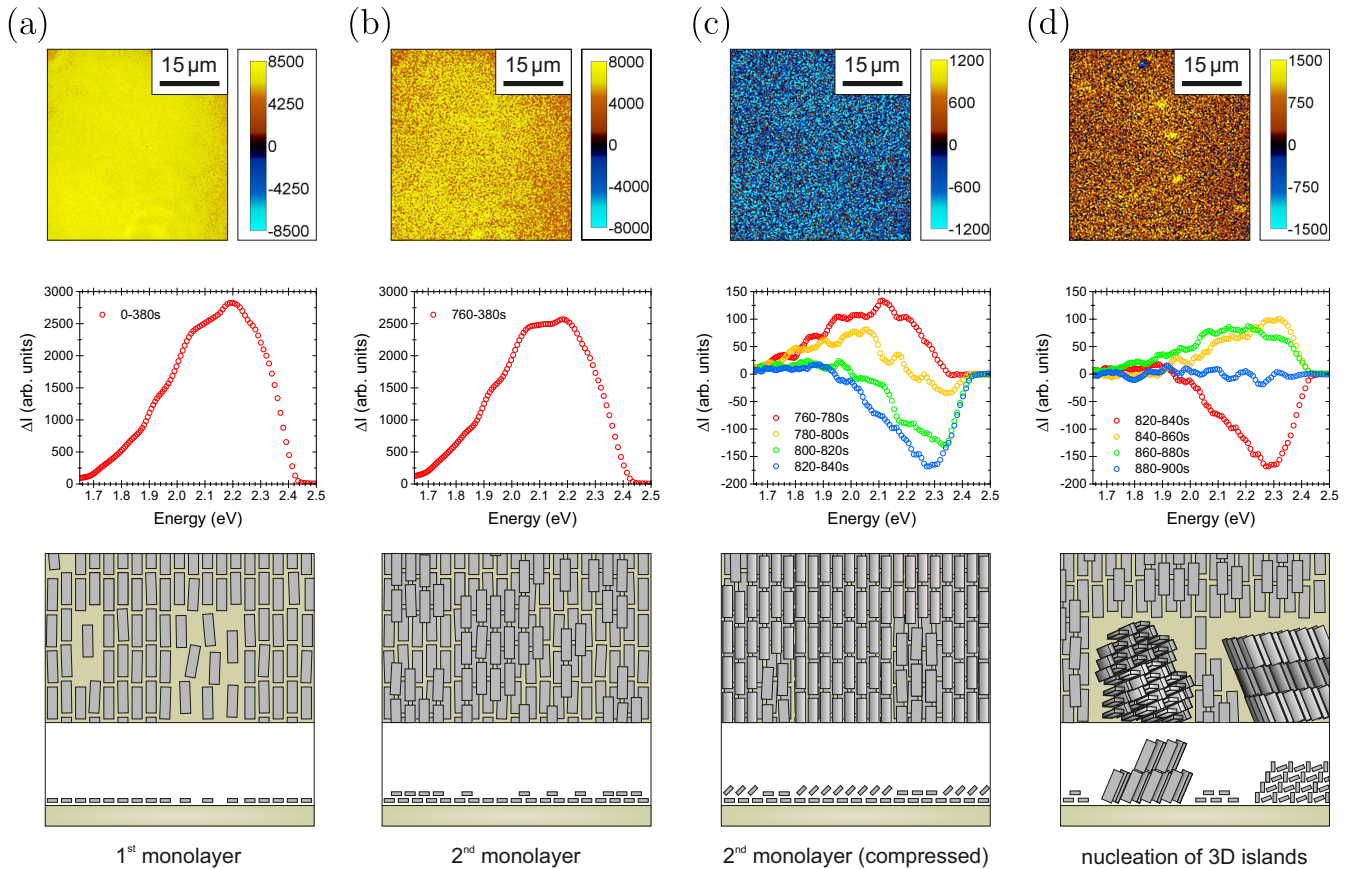
FIG. 3. The top row shows the differences between fluorescence microscopy images over growth stages (a) I, (b) II, (c) III, and (d) IV. The color scale goes from light blue (strongest fluorescence intensity loss) to yellow (maximum fluorescence intensity gain) as indicated in the color bar on the right. The second row shows incremental changes of the fluorescence spectra (ΔI) over the time frames given in the legends. The third row shows the proposed model for the molecular arrangement of α-6T (represented by gray cuboids) on the mica surface for the different growth stages.

[corresponding to the red area of Fig. 2(b)]. In the top image of column (a) of Fig. 3, the difference between the fluorescence microscopy image of the α-6T thin film after 380 s of deposition and the bare substrate is shown. It is easy to see that the intensity increase due to the α-6T thin film growth is homogeneous over the whole image area. This means that no structures larger than the diffraction limit are formed and suggests that α-6T molecules spread over the surface and wet the mica surface homogeneously. This argument is further supported by the fact that the spectral line shape of the difference between the corresponding fluorescence spectra [middle panel of column (a) in Fig. 3] is very close to that of the noninteracting α-6T molecules. This observation suggests that the lateral interaction between neighboring molecules is rather weak and thus the α-6T molecules are lying flat on the surface. Indeed, based on the deposition rate determined by the microbalance, a surface density of $\sim 6.5 \times 10^{13}$ molecules cm^{-2} of α-6T should be achieved after 380 s of deposition. This number coincides nicely with the surface density of a monolayer of flat-lying α-6T estimated from the van der Waals dimension of the molecule (see Fig. 1). The proposed arrangement of the α-6T molecules (each represented by a gray cuboid) close to the end of this growth stage is sketched at the bottom of column (a) of Fig. 3.

2. Growth stage II: Second-monolayer growth (380–760 s)

The growth of the second monolayer induces the splitting of the two curves in Fig. 2(b). The increase of the intensity slows down at 2.36 eV but accelerates at 1.94 eV, which suggests a spectral shift to lower energies. Indeed, the corresponding incremental change of the fluorescence spectrum that occurs during the deposition period between 380 and 760 s, which is plotted in the middle of column (b) of Fig. 3, confirms this redshift. This observation can be interpreted by the change of the dielectric environment of the α-6T molecules in the second monolayer relative to the ones within the first monolayer. Consistently, the corresponding variation of the fluorescence image [top image in column (b) of Fig. 3] is again homogeneous. The proposed molecular arrangement of α-6T molecules close to the end of this stage is shown at the bottom of column (b) in Fig. 3. The molecules in the second monolayer remain lying flat until the layer density reaches the critical coverage n_C.

3. Growth stage III: Wetting-layer compression (760–840 s)

The third growth stage sets in at the critical coverage n_C, when the fluorescence intensity at 2.36 eV starts to decrease slightly [see Fig. 2(b)]. The critical coverage n_C coincidences

with the upper limit of two monolayers consisting of flat-lying α-6T molecules. The detailed spectral evolution can be revealed by inspecting the incremental difference of the fluorescence spectra plotted in the middle panel of column (c) in Fig. 3. With the increase of α-6T coverage, a redshift of the fluorescence spectrum is observed. Subsequently, a gradual decrease of the fluorescence intensity centered around 2.36 eV occurs. The redshift and the reduction of the fluorescence intensity can be attributed to the reorientation of α-6T molecules in the second monolayer. Actually, the increase of the α-6T molecule density reduces the intermolecular distance, which in turn may induce a repulsive interaction between molecules. Consequently, the initially-flat-lying molecules reorient themselves into the edge-on conformation and the aromatic planes of the neighboring α-6T molecules become parallel to each other. The formation of this π-π stacking switches the intermolecular force between neighboring α-6T molecules from repulsive to attractive. It is well known that the optical absorption and emission properties of the molecular layers depend on the details of the arrangement of the molecules. Changing into edge-on conformation strongly enhances the overlapping between the aromatic planes of neighboring molecules which leads, typically, to a spectral redshift with a reduced fluorescence intensity [42]. The variation of the fluorescence image calculated by taking the difference between images recorded at 760 and 840 s shows a homogeneous reduction of the emission over the α-6T thin film which confirms the homogeneous compression over the second monolayer [top image in Fig. 3(c)]. Similar molecular reorientation induced by increasing the surface density has also been observed by Bröker *et al.* for the adsorption of hexaazatriphenylene-hexacarbonitrile molecules on the Ag(111) surface [43].

4. Growth stage IV: Onset of 3D nucleations (840–900 s)

Upon further deposition of α-6T molecules, the fluorescence intensity at 2.36 eV recovers within a short time interval between 840 and 900 s [blue area in Fig. 2(b)]. We attribute this observation to the decompression of the second monolayer due to the nucleation of 3D islands. The formation of the 3D α-6T islands extracts molecules from the surrounding wetting layer and spontaneously reduces the pressure (density of α-6T molecules) in the second monolayer. The reduction of the layer density leads to a reorientation of α-6T molecules in the second monolayer from edge-on back to flat lying. This can be seen even more clearly in column (d) of Fig. 3. In the differential image presented in the top panel, in addition to the increase of the intensity over the field of view, several bright spots as well as one dark spot can be resolved. We assign the bright spots to the needlelike 3D islands consisting of α-6T molecules with their long axis parallel to the substrate surface [30] and the dark spot to a 3D island of nearly-upright-standing molecules [30], respectively. As we have mentioned, the fluorescence signal observed here is associated to the HOMO-LUMO electronic transition with its transition dipole moment aligned along the long molecular axis. Due to the fact that emission propagates along the direction which is orthogonal to the transition dipole moment, and taking into consideration the finite angular aperture of the objective used ($\sim66°$), it becomes obvious that only the photoluminescence of α-6T molecules in the needlelike 3D islands can be collected under the current experiment setup, whereas the emission from the nearly-upright-standing α-6T molecules in the 3D islands with a contact plane of (100) [30] cannot be seen. Therefore, the 3D islands consisting of flat-lying and nearly-upright-standing α-6T molecules appear as bright and dark features, respectively, in the fluorescence microscopic images presented in this paper. Consequently, the image in column (d) of Fig. 3 reveals clearly the recovery of the fluorescence of the wetting layer and the formation of needlelike 3D islands (bright spots) as well as islands of upright-standing molecules (dark spot). This conclusion is further confirmed by the corresponding spectral difference which reveals the fluorescence increase with a spectral line shape close to the characteristic one of the second monolayer. The fact that the area covered by a standing island becomes even darker suggests the dewetting of the flat-lying molecules beneath.
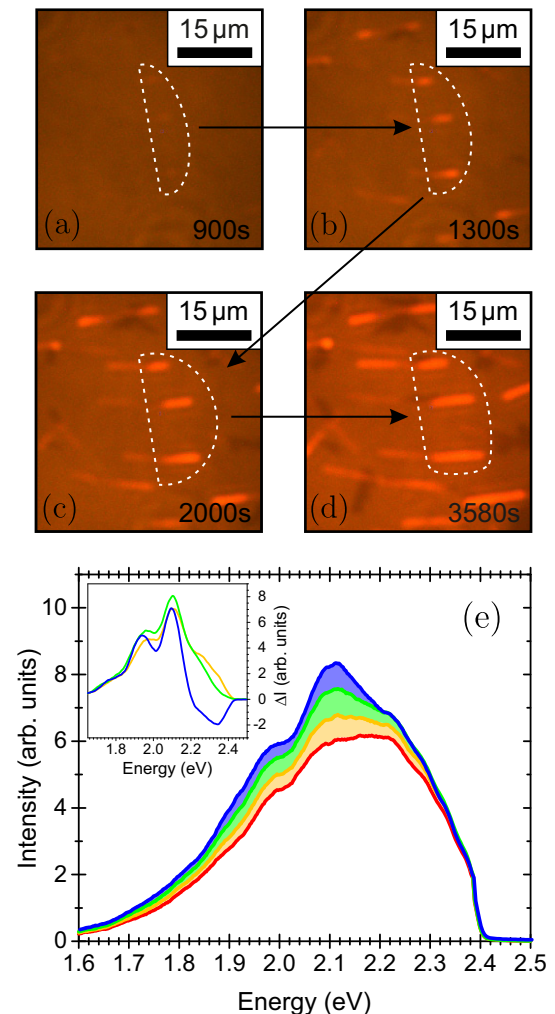

FIG. 4. Fluorescence microscopy images of the mica surface after (a) 900 s, (b) 1300 s, (c) 2000 s, and (d) 3580 s of deposition. Three needles in the center of the images are marked to clarify their growth in one direction with increasing deposition time. (e) Fluorescence spectra from the images in (a)–(d) shown in red, yellow, green, and blue, respectively. In the inset the change of the spectra is shown with the color of the line resembling the color of the respective area between the spectra in the main graph.
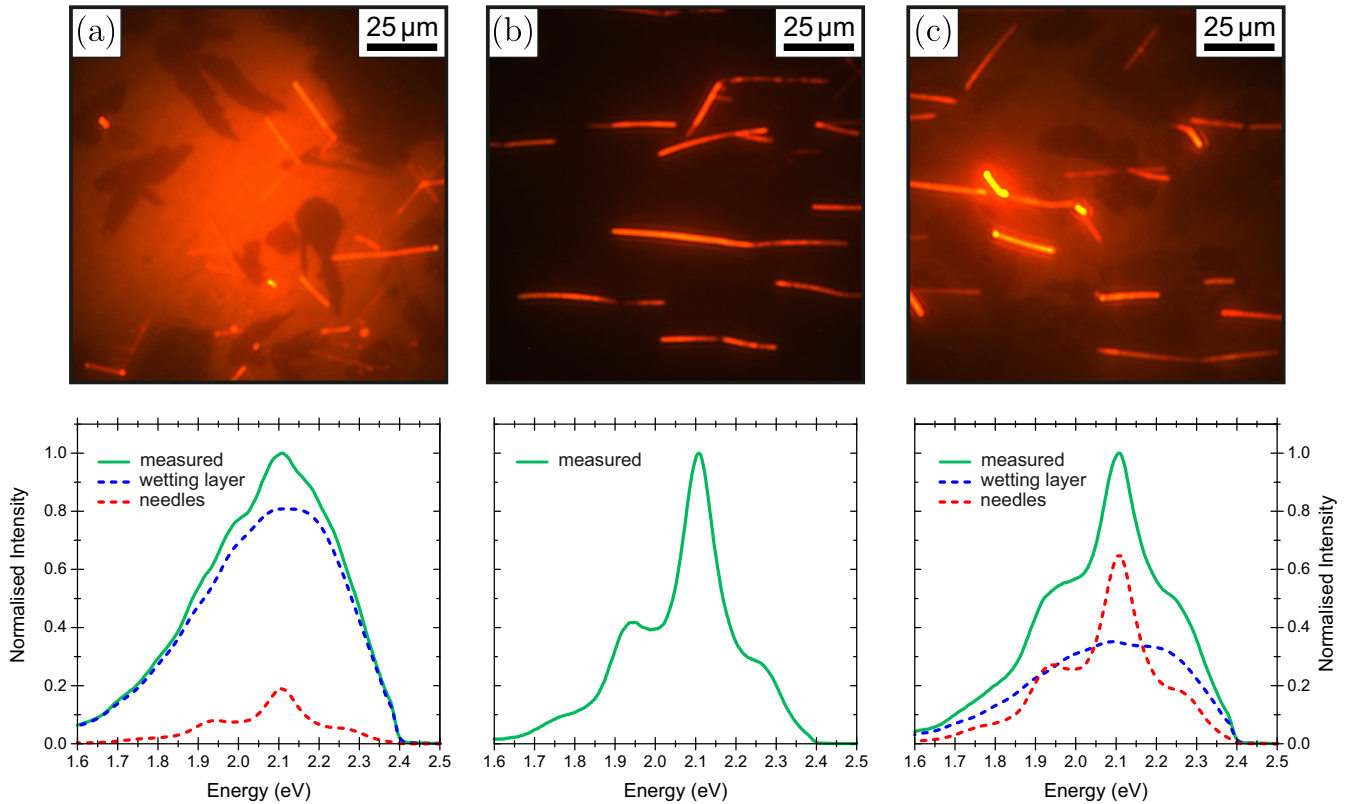
FIG. 5. Fluorescence microscopy images of a 6T thin film taken in (a) ultrahigh vacuum and (b) air. A fluorescence microscopy image of the same film after exposure to air and subsequent storage at approximately 10^{-6} mbar overnight can be seen in (c). The graphs underneath each image show the fluorescence spectra of the corresponding image as a green line. The blue dashed line, which resembles the spectrum of the wetting layer in the graphs under (a) and (c), can be calculated by subtracting the needle spectrum (dashed red line) from the green spectrum.

5. Growth stage V: Three-dimensional island growth

The detailed growth of 3D islands beyond 900 s of deposition time is presented in Fig. 4 using fluorescence microscope images recorded after 900 s [Fig. 4(a)], 1300 s [Fig. 4(b)], 2000 s [Fig. 4(c)], and 3580 s [Fig. 4(d)]. Increasing the deposition time, the growth of 3D islands consisting of flat-lying molecules can be clearly recognized by the formation and elongation of the bright needlelike features, whereas the dark areas representing 3D islands of nearly-upright-standing molecules extend simultaneously. The three islands, which are visible in Fig. 3(d) as bright spots, are encircled by a white dashed line. With the increase of deposition time, these bright spots gradually grow into long needles. Interestingly, the growth of these needles is always terminated at one end and is elongated into the other direction. Furthermore, the islands of upright-standing molecules always grow around the terminating end of one or several needles, suggesting that they may share a common nucleation center with one or more needlelike structures (see also Fig. 6). The corresponding fluorescence spectra recorded from the same field of view are plotted below in Fig. 4(e). Therein it can be seen that a new feature at 2.10 eV, which is an identifying characteristic of the α-6T crystals (see Fig. S2 in [36]), increases gradually with deposition time. This agrees fully with the growth of the α-6T needles observed in the fluorescence images. The differences between two subsequent spectra in Fig. 4(e), which reflect

the incremental changes of the fluorescence spectrum of the α-6T films with each deposition step (corresponding to the area between the spectra filled with the respective color), are plotted as an inset in the same figure. The different spectra closely resemble the fluorescence signal emitted by α-6T molecules from the crystalline phase [24,25,41], confirming the growth of needlelike structures. Additionally, the intensity increment at the short-wavelength side declines gradually and finally drops even into negative. Actually, the variation of the fluorescence intensity in this wavelength range is determined by a positive contribution from the accretion of α-6T molecules into the needles and a reduction due to the removal of α-6T molecules in the wetting layer upon the growth of islands of upright-standing molecules. The lagged enhancement of the dewetting effect observed here can be explained by a growth delay of islands containing upright-standing molecules relative to the needles as proposed in the literature [28–30,44].

B. Effect of air exposure on α-6T thin films

The influence of the air exposure to the morphology of α-6T thin films was investigated by monitoring the variation of the fluorescence emission from a thin film with a nominal thickness of approximately 2.3 nm. Upon air exposure, an obvious change was observed by both fluorescence spectroscopy and microscopy. Figure 5(a) shows the fluorescence
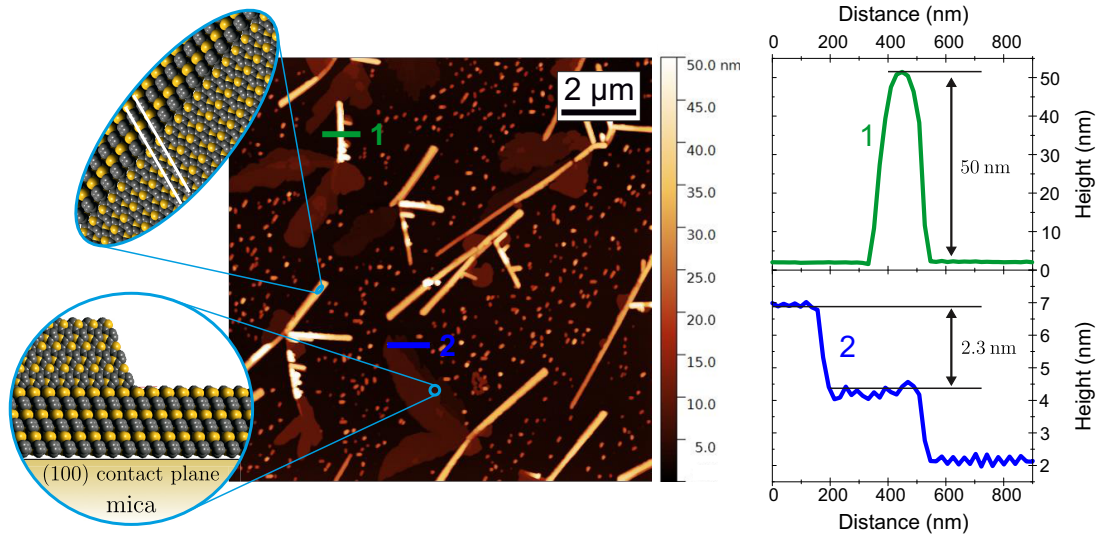
FIG. 6. Typical morphology of the α-6T thin films revealed using AFM. The nominal thickness of the α-6T thin film presented here is 2.3 nm. The molecular arrangement in the needles and the islands of upright-standing molecules are sketched in the insets; the white lines in the upper inset indicate the direction of the long molecular axis of α-6T molecules in the needlelike crystals. The line profiles crossing a needle (line 1) and an island of upright standing molecules (line 2) are plotted in the top and bottom panels of the right column, respectively.

microscopic image of the α-6T film recorded *in situ* before air exposure. The emission from both needlelike islands and the wetting layer in between is clearly visible. However, in the image taken from the same sample after venting the vacuum chamber by air [Fig. 5(b)], only α-6T needles still emit strongly, whereas the areas between them become completely dark. Subsequently, the vacuum chamber was pumped down to a pressure of approximately 10^{-6} mbar again and the fluorescence microscopy image recorded from the same sample after one night shows a partial recovery of the emission from the area between the α-6T needles [Fig. 5(c)]. We attribute the vanishing and the reappearance of the emission to the dewetting and partial recovering of the wetting layer, respectively. The normalized fluorescence spectra recorded simultaneously with each of these images are presented in the lower panels of Fig. 5 accordingly. The fluorescence spectrum recorded from the α-6T thin film in air [Fig. 5(b)], which is contributed exclusively by the α-6T needles, exhibits the characteristic line shape of bulk α-6T in the LT phase [24,25,41] (see Fig. S2 in [36]). The other two spectra recorded before venting [green line in Fig. 5(a)] and after reevacuation [green line in Fig. 5(c)], should be superpositions of the emissions from the needles and the wetting layer. Using the spectrum in Fig. 5(b) as the characteristic emission of α-6T needles, the contribution from the wetting layer can be deduced from the other two fluorescence spectra recorded in vacuum. The decomposed contributions from the wetting layer and needles are then plotted in Figs. 5(a) and 5(c) using blue and red dashed lines, respectively. Indeed, these blue spectra resemble the spectral line shape of the wetting layer recorded *in situ* during α-6T thin film growth. As expected, the fractional contribution of the wetting layer is only partially recovered after reevacuation [Fig. 5(c) vs Fig. 5(a)]. Despite the different intensities, the spectral line shape of the contribution of the wetting layer is similar in both cases, which agrees with the

proposed partial recovery of the wetting layer. The result presented here reveals that the α-6T wetting layer formed on the mica surface is unstable upon air exposure. The observed dewetting can be attributed to the change of surface/interface energies due to the adsorption of molecules from the air, e.g., water.

An *ex situ* atomic force microscopy (AFM) image (recorded in tapping mode) of a α-6T thin film with a nominal thickness of about 2.3 nm on mica acquired in air is presented in Fig. 6. It exhibits the typical morphology of α-6T thin films grown on mica substrates and is in full agreement with results previously reported by other groups [28,29]. Most importantly, in addition to the needles and the islands of upright-standing molecules, a large number of clusters distributed homogeneously on the surface in between can be identified. The exact composition and structure of these clusters is still unclear, however, it is reasonable to presume that the clusters are composed of the α-6T molecules which initially constitute the wetting layer. Indeed, according to the *ex situ* AFM and fluorescence microscopy measurements performed by Kankate *et al.* [29], the clusters are even formed for coverage lower than the critical coverage for 3D nucleation.

IV. CONCLUSION

In this work, real-time *in situ* fluorescence microscopy and fluorescence spectroscopy were applied to investigate the growth of α-6T thin films on muscovite mica. For this purpose, a home-built experimental setup was used, which enables the simultaneous *in situ* acquisition of microscopic and spectroscopic information of the fluorescence of organic molecules deposited on transparent substrates. In addition to the previously reported needlelike and flat islands of upright-standing molecules, the current *in situ* measurements reveal the formation of an α-6T wetting layer consisting of flat-lying

molecules on the mica surface. The characteristic fluorescence spectra of the wetting layer and needlelike 3D structures can clearly be distinguished in the presented fluorescence spectra. This establishes the base for the simultaneous probing of the growth of the wetting layer and the 3D islands by monitoring the fluorescence at the characteristic wavelengths. By exploiting the sensitive dependence of the fluorescence of the α-6T thin film on the molecular arrangement, the *in situ* dynamic study performed during the deposition of α-6T molecules reveals that the growth of α-6T on muscovite mica follows the Stranski-Krastanov growth mode with a wetting layer of two monolayer thickness.

The growth of the wetting layer goes through three stages, namely, formation of the first and the second monolayer of flat-lying molecules followed by a compression of the second monolayer leading to an edge-on molecular orientation. The compressed wetting layer relaxes upon the 3D nucleation and remains on the surface areas between the forthcoming 3D island. Due to the large supersaturation of α-6T on the surface, both needlelike features and the islands of upright-standing molecules are populated.

The instability of the wetting layer upon exposure to air is directly observed via a combination of *in situ* and *ex situ* fluorescence measurements and explains the absence of the α-6T wetting layer in previous works. In combination with AFM results obtained in air, it is argued that the α-6T molecules initially constituting the wetting layer incorporate themselves into the small clusters observed in air. In addition, the partial recovery of the wetting layer upon storage in high vacuum is documented. We attribute these dewetting (rewetting) processes to the variation of the surface/interface energy due to the adsorption (desorption) of air (most probably water molecules) on the mica surface.

The present work also demonstrates the power of real-time *in situ* fluorescence microscopy and fluorescence spectroscopy for investigating the details of the nucleation and growth of organic molecular structures on insulating substrates.

[1] S. R. Forrest, Nature (London) **428**, 911 (2004).

[2] M. Muccini, Nat. Mater. **5**, 605 (2006).

[3] S. R. Forrest, Chem. Rev. **97**, 1793 (1997).

[4] A. A. Virkar, S. Mannsfeld, Z. N. Bao, and N. Stingelin, Adv. Mater. **22**, 3857 (2010).

[5] F. Liscio, L. Ferlauto, M. Matta, R. Pfattner, M. Murgia, C. Rovira, M. Mas-Torrent, F. Zerbetto, S. Milita, and F. Biscarini, J. Phys. Chem. C **119**, 15912 (2015).

[6] G. Witte and C. Wöll, J. Mater. Res. **19**, 1889 (2004).

[7] F. Schreiber, Phys. Status Solidi A **201**, 1037 (2004).

[8] G. Hlawacek, P. Puschnig, P. Frank, A. Winkler, C. Ambrosch-Draxl, and C. Teichert, Science **321**, 108 (2008).

[9] A. Schöll, L. Kilian, Y. Zou, J. Ziroff, S. Hame, F. Reinert, E. Umbach, and R. H. Fink, Science **329**, 303 (2010).

[10] G. Koller, S. Berkebile, J. R. Krenn, F. P. Netzer, M. Oehzelt, T. Haber, R. Resel, and M. G. Ramsey, Nano Lett. **6**, 1207 (2006).

[11] A. Gerlach, S. Sellner, S. Kowarik, and F. Schreiber, Phys. Status Solidi A **205**, 461 (2008).

[12] T. Hosokai, A. Gerlach, A. Hinderhofer, C. Frank, G. Ligorio, U. Heinemeyer, A. Vorobiev, and F. Schreiber, Appl. Phys. Lett. **97**, 063301 (2010).

[13] F.-J. Meyer Zu Heringdorf, M. C. Reuter, and R. M. Tromp, Nature (London) **412**, 517 (2001).

[14] H. Marchetto, U. Groh, T. Schmidt, Rainer Fink, H.-J. Freund, and E. Umbach, Chem. Phys. **325**, 178 (2006).

[15] A. J. Fleming, S. Berkebile, T. Ules, and M. G. Ramsey, Phys. Chem. Chem. Phys. **13**, 4693 (2011).

[16] G. E. Thayer, J. T. Sadowski, F. Meyer zu Heringdorf, T. Sakurai, and R. M. Tromp, Phys. Rev. Lett. **95**, 256106 (2005).

[17] J. T. Sadowski, G. Sazaki, S. Nishikata, A. Al-Mahboob, Y. Fujikawa, K. Nakajima, R. M. Tromp, and T. Sakurai, Phys. Rev. Lett. **98**, 046104 (2007).

[18] G. Hlawacek, F. Khokhar, R. van Gastel, B. Poelsema, and C. Teichert, Nano Lett. **11**, 333 (2011).

[19] R. Forker and T. Fritz, Phys. Chem. Chem. Phys. **11**, 2142 (2009).

[20] L. D. Sun, G. Weidlinger, M. Denk, R. Denk, M. Hohage, and P. Zeppenfeld, Phys. Chem. Chem. Phys. **12**, 14706 (2010).

[21] M. Voigt, S. Dorsfeld, A. Volz, and M. Sokolowski, Phys. Rev. Lett. **91**, 026103 (2003).

[22] M. Pope and C. E. Swenberg, *Electronic Processes in Organic Crystals and Polymers*, 2nd ed. (Oxford Scientific, Oxford, 1999).

[23] F. Balzer and H.-G. Rubahn, Adv. Funct. Mater. **15**, 17 (2005).

[24] M. A. Loi, E. D. Como, F. Dinelli, M. Murgia, R. Zamboni, F. Biscarini, and M. Muccini, Nat. Mater. **4**, 81 (2005).

[25] E. D. Como, M. A. Loi, M. Murgia, R. Zamboni, F. Biscarini, and M. Muccini, J. Am. Chem. Soc. **128**, 4277 (2006).

[26] H. Zaglmayr, L. D. Sun, G. Weidlinger, S. M. Abd Al-Baqi, H. Sitter, and P. Zeppenfeld, Syn. Met. **161**, 271 (2011).

[27] C. Simbrunner, G. Hernandez-Sosa, F. Quochi, G. Schwabegger, C. Botta, M. Oehzelt, I. Salzmann, T. Djuric, A. Neuhold, R. Resel, M. Saba, A. Mura, G. Bongiovanni, A. Vollmer, N. Koch, and H. Sitter, ACS Nano **6**, 4629 (2012).

[28] F. Balzer, M. Schiek, H.-G. Rubahn, K. Al-Shamery, and A. Lützen, J. Vac. Sci. Technol. B **26**, 1619 (2008).

[29] L. Kankate, F. Balzer, H. Niehus, and H.-G. Rubahn, Thin Solid Films **518**, 130 (2009).

[30] C. Simbrunner, G. Hernandez-Sosa, M. Oehzelt, T. Djuric, I. Salzmann, M. Brinkmann, G. Schwabegger, I. Watzinger, H. Sitter, and R. Resel, Phys. Rev. B **83**, 115443 (2011).

[31] G. Horowitz, B. Bachet, A. Yassar, P. Lang, F. Demanze, J.-L. Fave, and F. Garnier, Chem. Mater. **7**, 1337 (1995).

[32] H. Poppa and A. G. Elliot, Surf. Sci. **24**, 149 (1971).

[33] K. G. Bhattacharyya, J. Electron Spectrosc. Relat. Phenom. **63**, 289 (1993).

[34] F. Balzer, L. Kankate, H. Niehus, and H.-G. Rubahn, Proc. SPIE **5925**, 59250A (2005).

[35] R. S. Becker, J. Seixas de Melo, A. L. Macanita, and F. Elisei, J. Phys. Chem. **100**, 18683 (1996).

[36] See Supplemental Material at http://link.aps.org/supplemental/10.1103/PhysRevMaterials.3.083402 for figures.

[37] W. Gebauer, A. Langner, M. Schneider, M. Sokolowski, and E. Umbach, Phys. Rev. B **69**, 155431 (2004).

[38] A. Langner, Y. Su, and M. Sokolowski, Phys. Rev. B **74**, 045428 (2006).

[39] J. Kerfoot, V. V. Korolkov, A. S. Nizovtsev, R. Jones, T. Taniguchi, K. Watanabe, I. Lesanovsky, B. Olmos, N. A. Besley, E. Besley, and P. H. Beton, J. Chem. Phys. **149**, 054701 (2018).

[40] R. R. Chance, A. Prock, and R. Silbey, Adv. Chem. Phys. **37**, 1 (1978).

[41] C. Simbrunner, F. Quochi, G. Hernandez-Sosa, M. Oehzelt, R. Resel, G. Hesser, M. Arndt, M. Saba, A. Mura, G. Bongiovanni, and H. Sitter, ACS Nano **4**, 6244 (2010).

[42] E. G. McRae and M. Kasha, J. Chem. Phys. **28**, 721 (1958).

[43] B. Bröker, O. T. Hofmann, G. M. Rangger, P. Frank, R.-P. Blum, R. Rieger, L. Venema, A. Vollmer, K. Müllen, J. P. Rabe, A. Winkler, P. Rudolf, E. Zojer, and N. Koch, Phys. Rev. Lett. **104**, 246805 (2010).

[44] C. Simbrunner, Semicond. Sci. Technol. **28**, 053001 (2013).